Unsupervised Method for Retinal Vessel Segmentation Based on Gabor Wavelet and Multiscale Line Detector

SYED AYAZ ALI SHAH[1], **AAMIR SHAHZAD**[1], **MUHAMMAD AMIR KHAN**[1],
CHENG-KAI LU[2]**, (Senior Member, IEEE), AND TONG BOON TANG**[2]**, (Senior Member, IEEE)**
[1]Department of Electrical and Computer Engineering, COMSATS University Islamabad, Abbottabad 22060, Pakistan
[2]Centre for Intelligent Signal and Imaging Research, Universiti Teknologi Petronas, Seri Iskandar 32610, Malaysia

Corresponding author: Tong Boon Tang (tongboon.tang@utp.edu.my)

ABSTRACT Eye and systemic diseases are known to manifest themselves in retinal vasculature. Segmentation of retinal vessel is one of the important steps in retinal image analysis. A simple unsupervised method based on Gabor wavelet and Multiscale Line Detector is proposed for retinal vessel segmentation. Vessels are enhanced by linear superposition of first scale Gabor wavelet image and complemented Green channel. Multiscale Line Detector is used to segment the blood vessels. Finally, a simple post processing scheme based on median filtering is deployed to remove false positives. The proposed scheme was evaluated with publicly available datasets called DRIVE, STARE and HRF, obtaining an accuracy of 0.9470, 0.9472, and 0.9559, and a sensitivity of 0.7421, 0.8004, and 0.7207, respectively. These results are comparable to the state-of-the-art methods, albeit with a simpler approach.

INDEX TERMS Blood vessel segmentation, color retinal images, Gabor wavelet, line detector, image processing, unsupervised method, image preprocessing.

I. INTRODUCTION

One of the important tasks in diagnosing different medical conditions such as diabetic retinopathy, cardiovascular diseases, and stroke is the segmentation of blood vessels in color medical images. To this end, different strategies have been devised. The strategies can be roughly grouped into i) multiscale, ii) matched filtering, iii) mathematical morphology, iv) hierarchical, v) model and vi) deep learning approach [1]. Furthermore, they can also be categorized into supervised and unsupervised algorithm. The prominent strategies based on multiscale are [2], [3]. Soares *et al.* [2] used Gabor wavelet transform with four scales (2,3,4,5) to account for different width sizes of blood vessel, and supervised classification. Nyugen *et al.* [4] proposed blood vessel segmentation using a multi-scale line detection based technique. The approach is an extension of the scheme based on single scale line detector and support vector machine [5]. Examples of filter based approach are [6]–[8] and

The associate editor coordinating the review of this manuscript and approving it for publication was Yongming Li [image].

mathematical morphology based are [9]–[11]. Retinal vessel segmentations based on hierarchical detections are [12], [13], model based approaches [14]–[16], and deep learning based schemes [13], [17]–[21].

One major challenge in retinal image analysis especially for accurate vessel detection is low and varying contrast. A method based on Gabor wavelet and multi-scale line detector is being proposed here. The Gabor wavelet transform presents high frequency precision in low frequencies and high spatial precision in high frequencies. In other words, the transform is suitable for detecting edges and other singularities in the image [22], [23]. By tuning its elongation and frequency parameters, Gabor wavelet transform can be used to detect elongated objects such as blood vessels (details can be found in [24]). However, detecting the edges in such way might result into central reflex type problem in the case of medium and fat vessels. Fig. 1 (a) and Fig. 1(b) describes the example of central reflex in colored and green channel, respectively. As the line-detection based approaches are shown to be effective in dealing with vessel central line reflex. Hence, using Gabor wavelet transform for edge enhancement
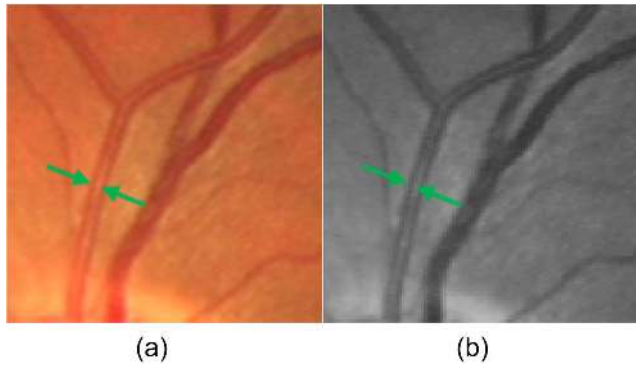
FIGURE 1. Central reflex in colored and green channel.

followed by application of line detector on enhanced image might overcome the central reflex problem and subsequently improve the vessel detection. Therefore, an unsupervised blood vessel segmentation method is proposed, which is based on image enhancement built on Gabor wavelet and line detector.

After image enhancement, the proposed approach uses multiple scale line detector and post-processing to overcome the central reflect problem and to remove false positives respectively. The proposed method obtains sensitivity of 0.7421, 0.8004 and 0.7207, and accuracy of 0.9470, 0.9472 and 0.9559 respectively on DRIVE, STARE and HRF datasets, which is comparable to the state-of-the-art methods. While on the DRIVE dataset, it takes less than 20 seconds on average per image, based on unoptimized Matlab scripts.

This paper is organized into five sections as follows: Section I, describes the introduction and literature review. Section II presents Gabor wavelet and Line Detector. Section III presents the materials and methods, while Section IV reports the results and discussion of the proposed methodology. Section V gives the conclusion of this work.

II. GABOR WAVELET AND LINE DETECTOR
The 2-D Gabor wavelet is defined as [2]:

$$\psi_G(x) = e^{(jk_0 x)} e^{(-\frac{1}{2}|Ax|^2)} \quad (1)$$

where A is 2 by 2 diagonal matrix and $A = [\varepsilon^{-1/2}, 1]$, $\varepsilon \geq 1$, its elongation in any desired direction. The parameter k_0 defines the frequency of the complex exponential. The filter is made elongated [24] by setting $\varepsilon = 4$ and k_0 is set to [0, 3], a low-frequency complex exponential with few significant oscillations perpendicular to the large axis of the wavelet. These two characteristics are especially suited for the detection of directional features and have been chosen in order to enable the transform to present stronger responses to pixels associated with the blood vessels. The other two key parameters of Gabor wavelet, after frequency and elongation, are scale and orientation. Scale selects the width of the elongated object while orientation is used for orientation of the objects. Vessels in the retinal image have different widths and can be in difference orientations. To accommodate all the

sizes of vessel, [2] used four scales i.e. 2, 3, 4 and 5. They used 18 different orientations and the highest response from all the orientations was kept [2].

Line Operator proposed by [5] was modified by [4] to include multiple scales by changing length of basic Line Detector/Operator and called it Multiscale Line Detector. The vessel central light reflex can be effectively dealt by the line detector. It is based on the logic that in inverted green channel, for vessel pixel, response will be high whereas for background it will be low (Eq. 2). In inverted green channel, when there is central light reflex, the pixels in the centre of vessel have comparatively lower intensities. Hence, they often give rise to misclassification. But in the case of line detector, they are recognized as vessel because winning line includes only a small number of 'central reflex' pixels. In inverted green channel, a window of size $W \times W$ pixels centered at each pixel position is used and average intensity (I_{mean}^W) is calculated. Lines with width of W and at angular resolution of 15° (12 lines in different directions) are passed through the centred pixels and the mean values of each line are calculated. The line with maximum value ($I^W max$) is the winning line. Response at a pixel is computed as [4]:

$$R_W = I_{max}^W - I_{mean}^W \quad (2)$$

Line detectors at multiple scales are achieved by

$$RW = I_{max}^L - I_{mean}^W \quad (3)$$

where $1 \leq L \leq W$. By changing the values of L, line detectors at different scales are obtained. In [4], angular resolution of 15° (12 different orientations), W equals to 15 pixels and line responses at 8 scales (from 1 to 15 with increment size of 2) are linearly combined.

III. MATERIAL AND METHODS
The proposed algorithm is assessed with publicly available color retinal images datasets called DRIVE [25], STARE [6] and HRF [26]. The DRIVE dataset consists of 40 images which is equally divided into training (20 images) and testing (20 images). The images are taken with three CCD cameras using 45-degree field of view (FOV). Each image is 768 by 584 pixels using 24 bits RGB color (8 bits per color plane). All images have FOV of around 540 pixels diameter, and each of them is accompanied by its mask image to delineate the FOV. The DRIVE dataset also provides the manually segmented images as the ground truth. Training images have single manual segmentation while for the test images there are two manual segmentations. Most of the researchers (as summarized in Table 1) use first manual segmentation to evaluate the performance of their algorithms. In this paper we use the first manual segmentations same as the other researchers do. STARE dataset on the other hand consists of 20 images with resolution of 700×605. The images are captured at 35° FOV and fifty percent of the images contain pathologies. Two different manual segmentations are provided for each image. However, the STARE dataset does not

TABLE 1. Results comparison.

Method / First author	Year	DRIVE				STARE				HRF			
		Acc	Se	Sp	MCC	Acc	Se	Sp	MCC	Acc	Se	Sp	MCC
2nd human observer	-	0.9473	0.7760	0.9724	0.7601	0.9354	0.8949	0.9390	0.7224	-	-	-	-
Our Method	**2019**	**0.9470**	**0.7421**	**0.9773**	**0.7525**	**0.9472**	**0.8004**	**0.9644**	**0.7294**	**0.9559**	**0.7202**	**0.9800**	**0.7244**
Supervised													
Staal [25]	2004	0.9442	0.6780	0.9830	0.7322	0.9516	0.6970	0.9810	-	-	-	-	-
Soares [2]	2006	0.9466	0.7283	0.9788	0.7488	0.9480	0.7197	0.9747	0.7200	-	-	-	-
Ricci-SVM[5]	2007	0.9424	-	-	-	0.9496	-	-	-	-	-	-	-
Marin[16]	2011	0.9452	0.7067	0.9725	-	0.9526	0.6944	0.9819	-	-	-	-	-
Li [17]	2016	0.9527	0.7569	0.9816	-	0.9628	0.7726	0.9844	-	-	-	-	-
Shah[1]	2017	0.9479	0.7205	0.9814	0.7529	-	-	-	-	-	-	-	-
Orlando[32]	2017	-	0.7897	0.9684	0.7556	0.7680	0.9738	-	0.7417	-	0.7874	0.9584	0.6897
Yang[27]	2019	0.9421	0.7560	0.9696	0.7365	0.9477	0.7202	0.9733	0.7045	0.9517	0.7915	0.9676	0.7125
Deep Learning													
Liskowski [28]	2016	0.9495	0.7763	0.9768	-	0.9566	0.7867	0.9754	-	-	-	-	-
Yan [18]	2018	0.9542	0.7653	0.9818	-	0.9612	0.7581	0.9846	-	0.9437	0.7881	0.9592	-
Alom [20]	2018	0.9556	0.7792	0.9813	-	0.9712	0.8298	0.9862	-				
Shin [21]	2019	0.9271	0.9382	0.9255	-	0.9378	0.9598	0.9352	-	0.9349	0.9546	0.9329	-
Unsupervised													
Zana [9]	2001	0.9377	-	-	0.7236								
Ricci-line[5]	2007	0.9329				0.9356	-	-	-	-	-	-	-
Nguyen [4]	2013	0.9407	0.7429	0.9700	0.7281	0.9324	-	-	-	-	-	-	-
Odstrcilik [26]	2013	0.9340	0.7060	0.9693	-	0.9341	0.7847	0.9512	-	0.9494	0.7794	0.9650	0.7065
Azzopardi [29]	2015	0.9442	0.7655	0.9704	0.7475								
Zhang [30]	2016	0.9476	0.7743	0.9725	-	0.9554	0.7791	0.9758	-	0.9556	0.7978	0.9717	0.7410
Oliveira [7]	2016	0.9464	0.8644	0.9556	0.7425	0.9532	0.8254	0.0353	0.7246	-	-	-	-
Rezaee [31]	2017	0.9463	0.7189	0.9793	-	0.9521	0.7202	0.9741	-	-	-	-	-

* It may be noted that values in the Table for [5] are taken from [4] while values for [26] are from [32].

provide separate training and test set unlike DRIVE dataset. In our evaluations we have used the first manual segmentation as the ground truth.

The third dataset, High-Resolution Fundus (HRF) Image Database, is also adopted to evaluate the performance of the proposed algorithm. This dataset consists of 45 images and are grouped into three subcategories of each contains 15 images of healthy, diabetic retinopathy and glaucoma. The images have a resolution of 3504×2336 and FOV of 60°. The dataset is also provided with single manual segmentation and mask for each image. The parameter values were estimated using the training images provided by DRIVE dataset. In case of STARE dataset, there is no standardized procedure available in the literature for dividing the images into train and test dataset [32], so we used five images for parameter estimation. For HRF dataset similar to [32], the first five images from each group were utilized for parameter estimation.

Fig. 2 describes the flow diagram of the proposed vessel segmentation technique. The proposed methodology consists of: a). image preprocessing based on Gabor wavelet, b).

candidate blood vessel extraction based on Multiscale Line Detector, and c). Post processing.

a. Image Preprocessing: Blood vessels appear as dark objects in green channel. They have the highest contrast in green channel. However, color retinal images suffer from low and varying contrast, which makes it difficult to extract blood vessel based on intensity alone. To overcome this problem, we propose the linear superposition of Gabor wavelet-based scheme at single scale (first scale only) and complemented green channel. We set the elongation and frequency parameter values respectively to $\epsilon = 4$ and $k_0 = [0, 3]$, so as to detect the elongated objects and filter out the other objects and noise. Gabor wavelet using first scale only enhanced the fine vessels and the edges of the wide vessels. From 0° to 170° in the steps of 10, Gabor wavelet was taken, and the maximum response was kept among 18 different orientations. The image containing the maximum responses out of 18 different orientations was added with the complemented green channel to obtain the preprocessed image. This resulted in better contrast for elongated objects such as vessels. Fig. 2, top row second image is the green channel and the one on the right is resulting
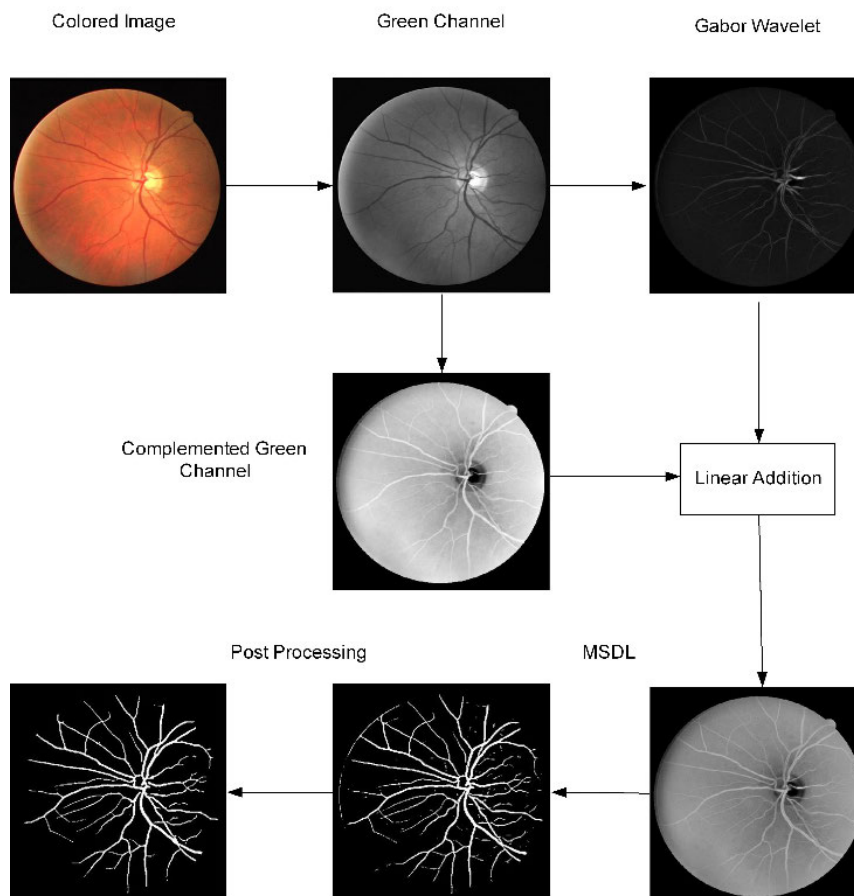
FIGURE 2. Flow diagram of the proposed system.

image after Gabor wavelet taken in the described way. The image on the right in bottom row of Fig. 1 shows the described preprocessed mage.

b. Candidate blood vessel extraction based on Multiscale Line Detector: During the preprocessing, we took Gabor wavelet response at first scale only, thus the wide vessel might suffer from the central reflex type situation. To overcome this issue, we proposed to use Multiscale Line Detector, an effective technique in central light reflex situation. We used $W = 13$, 17 and 45 pixels and line responses at 7, 9 and 23 scales were linearly combined respectively for DRIVE, STARE and HRF dataset. The angular resolution was 15° (12 lines in different directions). After the application of Multiscale Line Detector, images were thresholded to obtain the binarized images. After threshold, filling was applied to fill the one-pixel gap. The resulting image is shown in Fig. 2, in the middle of the bottom row.

c. Post-processing: After application of Multiscale Line Detector, there were false positives around the Region of Interest (ROI) boundary, in the optic disc (OD) region and at the edges of the medium and fine vessels. To remove these false positives, we proposed a postprocessing scheme in which background was calculated using a median filter of the size of 15×15, 17×17 and 45×45, respectively

for DRIVE, STARE and HRF datasets and removed from the green channel. The background removed image was further median filtered using a 3x3 array to obtain a smoothed background removed image denoted by GrnSBKRMImg. In the GrnSBKRMImg, pixels were bright both for the OD region and ROI boundary while blood vessels and other dark objects such as hemorrhages appear dark, as could be clearly observed in Fig. 3. Even most of the blood vessels inside OD became dark, as shown in Fig. 3. Therefore, to remove such false positives, we presumed that vessels having width equal to greater than 2 pixels had lower intensity values than those falsely detected objects such as from ROI and OD region. Thus, using intensity values in GrnSBKRMImg all the vessels having width 2 pixels or more were checked and classified into non-vessels if their intensity values were higher than the specified threshold. Finally, all those objects which were 100 pixels or less in case of DRIVE dataset and 500 pixels for STARE dataset and 2500 pixels for HRF dataset, and having intensity greater than specified threshold than the mean intensity in GrnSBKRMImg are also removed. In this way, we were able to get rid from most of the false positives contributed by ROI and OD region. Shown in Fig. 2, the first image from left side in bottom row is the final image obtained after postprocessing.
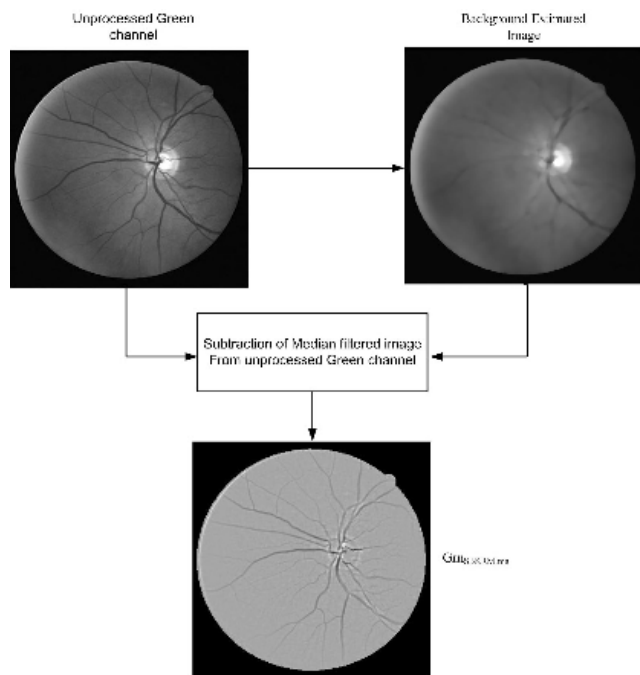
FIGURE 3. Pre-processing to obtain GrnSBKRMImg.

FIGURE 4. ROC curve on DRIVE dataset.

To evaluate the performance of the proposed system, the following parameters are used:

i. True Positive Rate (TPR) or Sensitivity.
ii. False Positive Rate (FPR).
iii. Accuracy (ACC).
iv. Receiver Operating Characteristics Curve (ROC), for DRIVE dataset only.
v. Matthews Correlation Coefficient (MCC).

These parameters are mathematically defined using Eq. 4-7 except ROC which is a curve, obtained by plotting sensitivity along y-axis and FPR on x-axis. These parameters were calculated for each pixel inside the ROI region using the first manual segmentation as a gold standard, which was used by the authors in comparison Table 1. Definitions:

TP is true positive, if a pixel detected by our proposed system as blood vessel and be consistent with its identification by the ground truth.

FP is false positive, if the proposed system determines non-vessel pixels as vessel pixels.

TN is true negative, if the proposed system detects a pixel as non-blood and ground truth also indicates it as a non-vessel pixel.

FN is false negative, if a pixel recognised by the proposed system is a non-blood pixel whereas ground truth identifies it as a vessel pixel.

MCC was introduced by [21] which measures the quality of binary classification. It is also good for the case where the two classes are imbalance as is the case of retinal vessel segmentation. Its value will be +1 when the system does not make any mistake i.e. ideal system no false positive and no false negative. Similarly, its value will be −1, if all the values are false positives and false negatives and no true positive and true negative. As a result, the MCC value closer
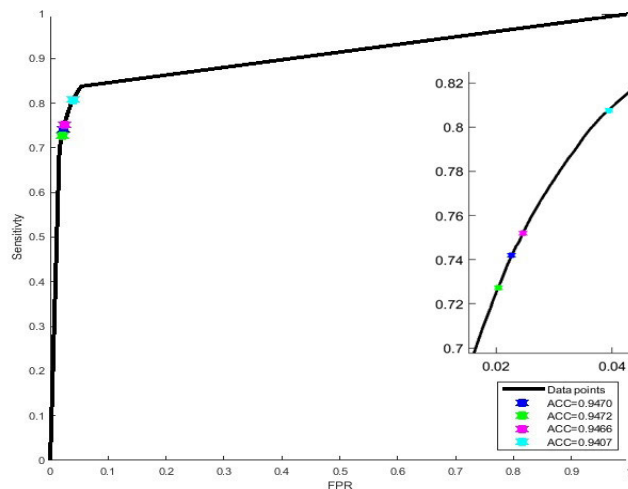
to +1 indicates a better classification system.

$$TPR = TP/(TP + FN) \tag{4}$$

$$FPR = 1 - TN/(FP + TN) \tag{5}$$

$$ACC = (TP + TN)/(TP + TN + FP + FN) \tag{6}$$

$$MCC = (TP \times TN - FP \times FN)/$$
$$\sqrt{((TP + FP)(TP + FN)(TN+FP)(TN+FN))} \tag{7}$$

IV. RESULTS AND DISCUSSION

The results of the proposed system using DRIVE, STARE and HRF datasets are described in Table 1. Fig. 4 shows the ROC of the proposed blood vessel segmentation scheme using DRIVE dataset. We achieved an accuracy of 0.9470, sensitivity of 0.7421, false positive rate of 0.0227, and MCC of 0.7525 on DRIVE dataset. As described in the previous section that the MCC value indicates quality of binary classifier such as blood vessel segmentation system and for the ideal system it will be +1. The proposed system achieved MCC value of 0.7525 which is better than all the unsupervised methods presented in Table 1 and very near to the 2nd Observer (0.7601). The scheme was very effective for wide vessel detection and we have negligible false positives around the wide blood vessels. Although the proposed scheme is good at detecting medium wide and fine vessels, it still suffers from over segmentation in the case of fine and medium wide vessels.

The proposed system could detect blood vessels in OD region and produced very few false positives in optic region and ROI region. Fig. 5 shows the two extreme cases of results of the proposed system. The upper row in Fig. 5 shows a case where it achieved the best accuracy while bottom row presents the case where it achieved the worst accuracy. In Fig. 5, the first column is colored image, second column is the ground truth, third column is segmented blood vessels while in fourth column the same segmented image as in column three where black pixels are true negative (TN), white are the true positives (TP), red pixels are false positives (FP)
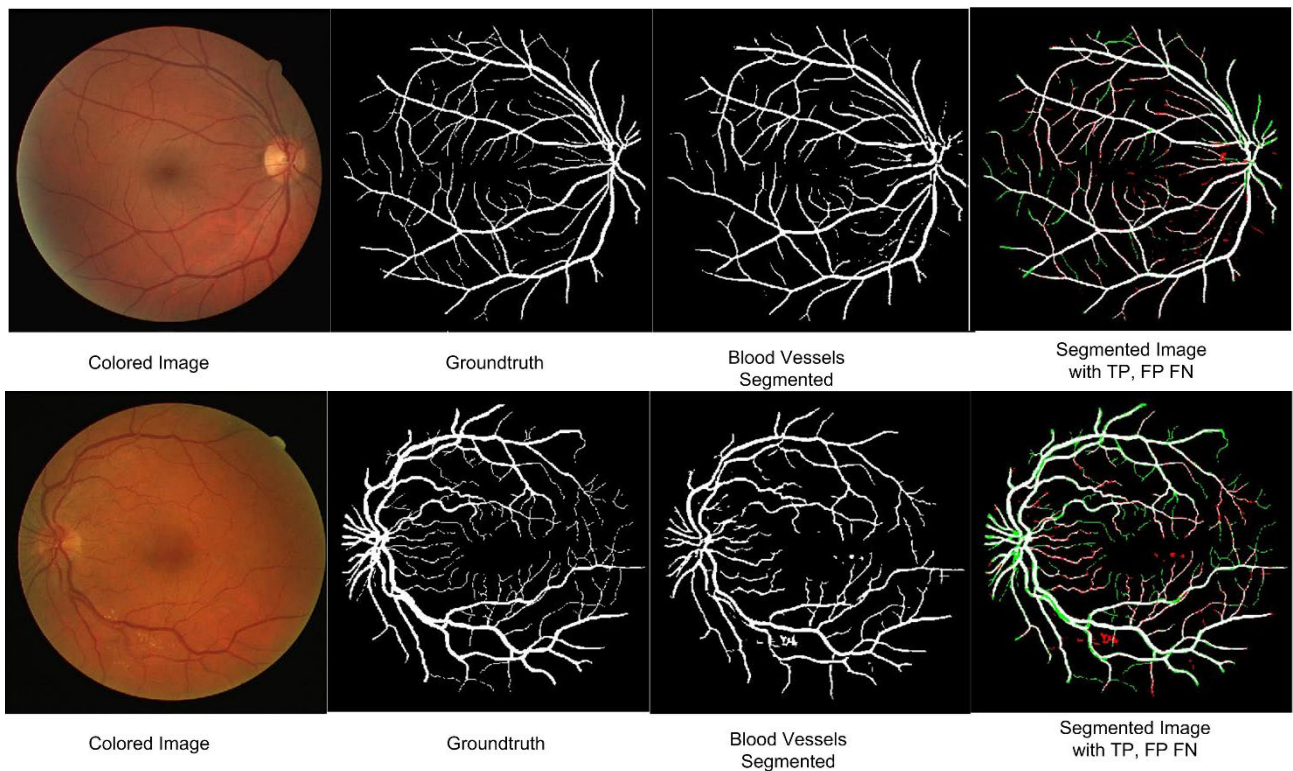
| Colored Image | Groundtruth | Blood Vessels Segmented | Segmented Image with TP, FP FN |

| Colored Image | Groundtruth | Blood Vessels Segmented | Segmented Image with TP, FP FN |

FIGURE 5. Results of proposed system on DRIVE dataset describing best (top row) and worst (bottom row) case accuracies respectively. Colored in red are the FP pixels while green are the FN pixels.
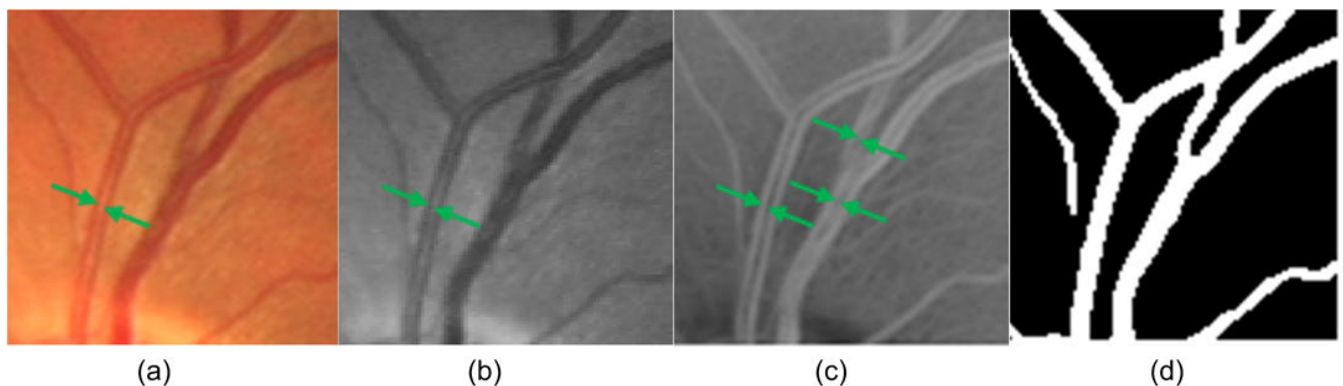

(a)   (b)   (c)   (d)

FIGURE 6. (a) and (b) shows in color and green channel the central reflex while (c) is obtained after image preprocessing and image (d) is the blood vessel segmented image.

and green are the missed vessel pixels (FN). It can be noticed that in both of the images shown in Fig. 5, the proposed system was able to detect most of the blood vessels inside OD region. The false positives were mostly from over segmentation of medium and fine vessels and those from lesions both bright and dark. Fig. 6 shows the central reflex problem, (a) and (b) shows a patch containing central reflex in color and green channel respectively. While shown in Fig. 6 (c) is the same patch but after image preprocessing, it is quite clear that now the fat vessels have additional central reflex type problems due to using the Gabor wavelet at single scale. This additional central reflex as well as the one already presents in the patch are well dealt by the Multiscale line detector as shown in Fig. 6 (d), which describes the blood vessel

extracted from the patch. It is quite clear that the central reflex issue was solved by the Multiscale Line Detector. The performance comparison of the proposed method in terms of execution time for DRIVE dataset is presented in Table 2. The proposed method processes an image in less than 20 seconds on average on unoptimized matlab code using core i5 with 6 GB RAM.

The proposed system achieved high sensitivity on STARE dataset with comparable accuracy as described in Table 1. The accuracy and MCC values were, respectively, 0.9472 and 0.7294 which were higher than the human observer. Fig. 7 shows the best case and the worst-case accuracies achieved by the proposed system on STARE dataset. Similarly, on HRF dataset, the proposed system achieved very
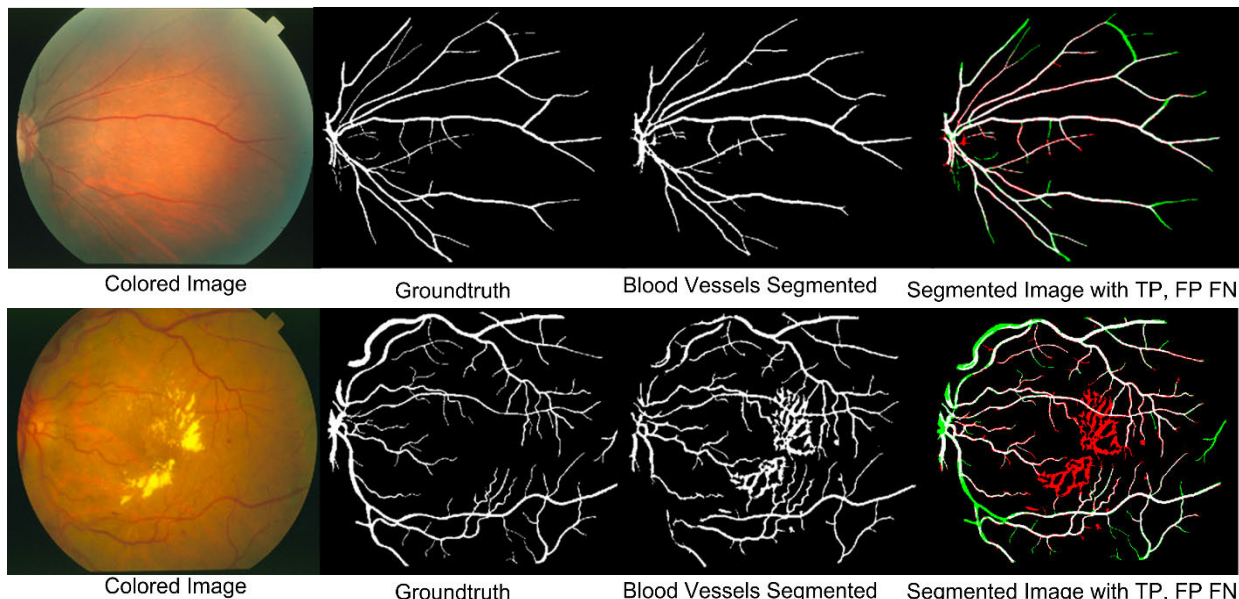
FIGURE 7. Results of proposed system on STARE dataset describing best (top row) and worst (bottom row) case accuracies respectively. Colored in red are the FP pixels while green are the FN pixels.

FIGURE 8. Results of proposed system on HRF dataset describing best (top row) and worst (bottom row) case accuracies respectively. Colored in red are the FP pixels while green are the FN pixels.
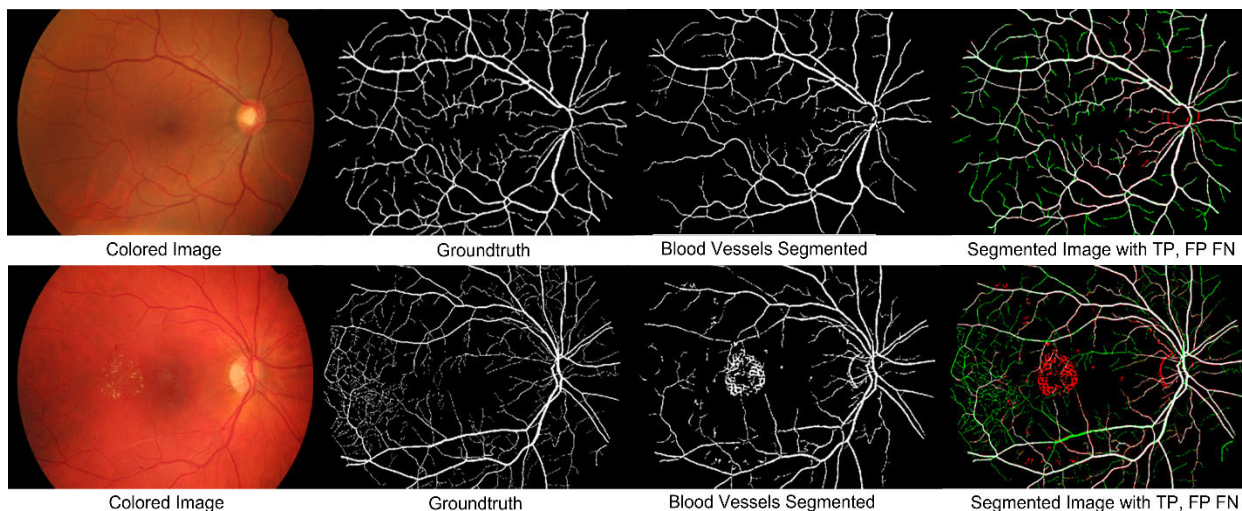
TABLE 2. Performance of segmentation in terms of execution time for DRIVE dataset.

Method	Running time
Second observer	7200s
Staal et al. [20]	900 s
Soares et al. [2]	190 s (9 h for training)
Multiscale Line Detector [4]	2.5 s
Proposed method	Less than 20 s

* It may be noted that values in the Table for [2,4,20] are taken from **[4].**

TABLE 3. HRF dataset.

Image Type (mean values)	Accuracy	Sensitivity	Specificity
DR	0.9512	0.7243	0.9718
Glaucoma	0.9591	0.7395	0.9786
Healthy	0.9575	0.6983	0.9898
Overall Mean	0.9559	0.7207	0.9800

high accuracy and specificity reflecting the strength of the technique. It achieved overall mean accuracy of 0.9559 and overall mean MCC value of 0.7244. Fig. 8 shows the best case and the worst-case accuracies achieved by the proposed

system on HRF dataset. It is clear from the Fig.7 and 8 that the proposed technique was not effective in dealing with pathological images which are detected as false positives. The mean values on individual groups i.e. DR, Glaucoma and Healthy images are presented in Table 3. It can be seen that the proposed technique achieved the highest mean accuracy

and mean sensitivity on Glaucoma group while it achieved the highest mean specificity of 0.9898 on healthy images of HRF dataset. In general, the proposed system demonstrated that it could detect the thick vessels with high accuracy and negligible false positives in all the three datasets, while in case of fine vessels the proposed system had a lower sensitivity and many fine vessels were missed.

V. CONCLUSION

In this paper, a novel unsupervised method for blood vessel segmentation was proposed. Single scale Gabor wavelet and Multiscale Line Detector were utilized to extract the blood vessel. A post processing scheme was devised based on intensity feature to differentiate between wide blood vessels and false positives due to the OD boundary and ROI boundary. The effectiveness of the proposed technique was tested on the datasets of DRIVE, STARE and HRF. The results showed that the proposed technique was equally effective on comparatively low-resolution dataset such as DRIVE, on a challenging dataset STARE and on a high resolution dataset (HRF). The proposed scheme is better in terms of both accuracy and sensitivity than the supervised method of Soares *et al.* [2] on DRIVE dataset. It can be noticed from the Table 2 that the proposed method took less time than [2]. Overall, it achieved 0.9470 at a similar accuracy level as the state-of-the-art methods while on average it took less than 20 seconds per image using unoptimized Matlab scripts.

REFERENCES

[1] S. A. A. Shah, T. B. Tang, I. Faye, and A. Laude, "Blood vessel segmentation in color fundus images based on regional and Hessian features," *Graefe's Arch. Clin. Exp. Ophthalmol.*, vol. 255, no. 8, pp. 1525–1533, 2017.

[2] J. V. B. Soares, J. J. G. Leandro, R. M. Cesar, H. F. Jelinek, and M. J. Cree, "Retinal vessel segmentation using the 2-D Gabor wavelet and supervised classification," *IEEE Trans. Med. Imag.*, vol. 25, no. 9, pp. 1214–1222, Sep. 2006.

[3] M. S. Miri and A. Mahloojifar, "Retinal image analysis using curvelet transform and multistructure elements morphology by reconstruction," *IEEE Trans. Biomed. Eng.*, vol. 58, no. 5, pp. 1183–1192, May 2011.

[4] U. T. V. Nguyen, A. Bhuiyan, L. A. F. Park, and K. Ramamohanarao, "An effective retinal blood vessel segmentation method using multi-scale line detection," *Pattern Recognit.*, vol. 46, no. 3, pp. 703–715, 2013.

[5] E. Ricci and R. Perfetti, "Retinal blood vessel segmentation using line operators and support vector classification," *IEEE Trans. Med. Imag.*, vol. 26, no. 10, pp. 1357–1365, Oct. 2007.

[6] A. D. Hoover, V. Kouznetsova, and M. Goldbaum, "Locating blood vessels in retinal images by piecewise threshold probing of a matched filter response," *IEEE Trans. Med. Imag.*, vol. 19, no. 3, pp. 203–210, Mar. 2000.

[7] W. S. Oliveira, J. V. Teixeira, T. I. Ren, G. D. C. Cavalcanti, J. Sijbers, "Unsupervised retinal vessel segmentation using combined filters," *PLoS ONE*, vol. 11, no. 2, 2016, Art. no. e0149943.

[8] B. Zhang, L. Zhang, L. Zhang, and F. Karray, "Retinal vessel extraction by matched filter with first-order derivative of Gaussian," *Comput. Biol. Med.*, vol. 40, no. 4, pp. 438–445, 2010.

[9] F. Zana and J. C. Klein, "Segmentation of vessel-like patterns using mathematical morphology and curvature evaluation," *IEEE Trans. Image Process.*, vol. 10, no. 7, pp. 1010–1019, Jul. 2001.

[10] M. M. Fraz, S. A. Barman, P. Remagnino, A. Hoppe, A. Basit, B. Uyyanonvara, A. R. Rudnicka, and C. G. Owen, "An approach to localize the retinal blood vessels using bit planes and centerline detection," *Comput. Methods Programs Biomed.*, vol. 108, no. 2, pp. 600–616, 2012.

[11] A. M. Mendonca and A. Campilho, "Segmentation of retinal blood vessels by combining the detection of centerlines and morphological reconstruction," *IEEE Trans. Med. Imag.*, vol. 25, no. 9, pp. 1200–1213, Sep. 2006.

[12] S. Roychowdhury, D. D. Koozekanani, and K. K. Parhi, "Blood vessel segmentation of fundus images by major vessel extraction and subimage classification," *IEEE J. Biomed. Health Inform.*, vol. 19, no. 3, pp. 1118–1128, May 2015.

[13] S. Wang, Y. Yin, G. Cao, B. Wei, Y. Zheng, and G. Yang, "Hierarchical retinal blood vessel segmentation based on feature and ensemble learning," *Neurocomputing*, vol. 149, pp. 708–717, Feb. 2015.

[14] Y. Zhao, Y. Liu, X. Wu, S. P. Harding, Y. Zheng, "Retinal vessel segmentation: An efficient graph cut approach with retinex and local phase," *PLoS ONE*, vol. 10, no. 4, 2015, Art. no. e0122332.

[15] K. A. Vermeer, F. M. Vos, H. G. Lemij, and A. M. Vossepoel, "A model based method for retinal blood vessel detection," *Comput. Biol. Med.*, vol. 34, no. 3, pp. 209–219, 2004.

[16] D. Marin, A. Aquino, M. E. Gegundez-Arias, and J. Bravo, "A new supervised method for blood vessel segmentation in retinal images by using gray-level and moment invariants-based features," *IEEE Trans. Med. Imag.*, vol. 30, no. 1, pp. 146–158, Jan. 2011.

[17] Q. Li, B. Feng, L. Xie, P. Liang, H. Zhang, and T. Wang, "A cross-modality learning approach for vessel segmentation in retinal images," *IEEE Trans. Med. Imag.*, vol. 35, no. 1, pp. 109–118, Jan. 2016.

[18] Z. Yan, X. Yang, and K.-T. Cheng, "Joint segment-level and pixelwise losses for deep learning based retinal vessel segmentation," *IEEE Trans. Biomed. Eng.*, vol. 65, no. 9, pp. 1912–1923, Sep. 2018.

[19] D. Maji, A. Santara, P. Mitra, and D. Sheet, "Ensemble of deep convolutional neural networks for learning to detect retinal vessels in fundus images," 2016, *arXiv:1603.04833*. [Online]. Available: https://arxiv.org/abs/1603.04833

[20] M. Z. Alom, M. Hasan, C. Yakopcic, T. M. Taha, and V. K. Asari, "Recurrent residual convolutional neural network based on u-net (R2U-net) for medical image segmentation," 2018, *arXiv:1802.06955*. [Online]. Available: https://arxiv.org/abs/1802.06955

[21] S. Y. Shin, S. Lee, I. D. Yun, and K. M. Lee, "Deep vessel segmentation by learning graphical connectivity," *Med. Image Anal.*, vol. 58, Dec. 2019, Art. no. 101556.

[22] S. Mallat and W. L. Hwang, "Singularity detection and processing with wavelets," *IEEE Trans. Inf. Theory*, vol. 38, no. 2, pp. 617–643, Mar. 1992.

[23] S. Mallat and S. Zhong, "Characterization of signals from multiscale edges," *IEEE Trans. Pattern Anal. Mach. Intell.*, vol. 14, no. 7, pp. 710–732, Jul. 1992.

[24] J. V. B. Soares and R. M. Cesar, Jr., "Segmentation of retinal vasculature using wavelets and supervised classification: Theory and implementation," in *Automated Image Detection of Retinal Pathology*. Boca Raton, FL, USA: CRC Press, 2009, pp. 239–286.

[25] J. Staal, M. D. Abramoff, M. Niemeijer, M. A. Viergever, and B. van Ginneken, "Ridge-based vessel segmentation in color images of the retina," *IEEE Trans. Med. Imag.*, vol. 23, no. 4, pp. 501–509, Apr. 2004.

[26] J. Odstrcilik, R. Kolar, A. Budai, J. Hornegger, J. Jan, J. Gazarek, T. Kubena, P. Cernosek, O. Svoboda, and E. Angelopoulou, "Retinal vessel segmentation by improved matched filtering: Evaluation on a new high-resolution fundus image database," *IET Image Process.*, vol. 7, no. 4, pp. 373–383, Jun. 2013.

[27] Y. Yang, F. Shao, Z. Fu, and R. Fu, "Discriminative dictionary learning for retinal vessel segmentation using fusion of multiple features," *Signal, Image Video Process.*, vol. 13, pp. 1529–1537, Nov. 2019.

[28] P. Liskowski and K. Krawiec, "Segmenting retinal blood vessels with deep neural networks," *IEEE Trans. Med. Imag.*, vol. 35, no. 11, pp. 2369–2380, Nov. 2016.

[29] G. Azzopardi, N. Strisciuglio, M. Vento, and N. Petkov, "Trainable COS-FIRE filters for vessel delineation with application to retinal images," *Med. Image Anal.*, vol. 19, no. 1, pp. 46–57, Jan. 2015.

[30] J. Zhang, B. Dashtbozorg, E. Bekkers, J. P. W. Pluim, R. Duits, and B. M. T. H. Romeny, "Robust retinal vessel segmentation via locally adaptive derivative frames in orientation scores," *IEEE Trans. Med. Imag.*, vol. 35, no. 12, pp. 2631–2644, Dec. 2016.

[31] K. Rezaee, J. Haddadnia, and A. Tashk, "Optimized clinical segmentation of retinal blood vessels by using combination of adaptive filtering, fuzzy entropy and skeletonization," *Appl. Soft Comput.*, vol. 52, pp. 937–951, Mar. 2017.

[32] J. I. Orlando, E. Prokofyeva, and M. B. Blaschko, "A discriminatively trained fully connected conditional random field model for blood vessel segmentation in fundus images," *IEEE Trans. Biomed. Eng.*, vol. 64, no. 1, pp. 16–27, Jan. 2017.

• • •